

## Axial oxygen-centered lattice instabilities in $\text{YBa}_2\text{Cu}_3\text{O}_7$ : An application of the analysis of extended x-ray-absorption fine structure in anharmonic systems

J. Mustre de Leon, S. D. Conradson, I. Batistić, A. R. Bishop, I. D. Raistrick, M. C. Aronson,\* and  
F. H. Garzon

*Electronics Research and Theoretical Condensed Matter Physics Groups,  
Los Alamos National Laboratory, Los Alamos, New Mexico 87545*

(Received 26 December 1990; revised manuscript received 6 May 1991)

Analysis of polarized copper  $K$ -edge extended x-ray-absorption fine-structure (EXAFS) measurements on  $\text{YBa}_2\text{Cu}_3\text{O}_7$  for temperatures  $10 \leq T_{\text{nom}} \leq 105$  K indicates that the axial oxygen moves in a double-well potential which softens within a fluctuation region associated with the onset of superconductivity in this material. This fluctuation follows from the coupling between the phonons derived from this double-well potential and the superconducting order parameter. The advantages of EXAFS compared to crystallographic measurements in discerning these aspects of the local structure are discussed. Metrical parameters and the characteristics of the potential are determined by curve fits of the EXAFS. This method is based on the calculation of radial distribution functions from selected model potentials, the forms of which are determined along with the absorber-scatterer distance, scatterer type, and number, by optimization of fits of the experimental data with the EXAFS calculated from these parameters. Unlike perturbative treatments, this approach is ideally suited for highly anharmonic systems because the putative potential can be a very close approximation to the real one and it also offers the advantage of providing dynamical information not available through perturbative treatments.

### I. INTRODUCTION

We have recently presented an analysis of polarized extended x-ray-absorption fine-structure (EXAFS) data on oriented  $\text{YBa}_2\text{Cu}_3\text{O}_7$  powders as a function of temperature which indicates that a lattice fluctuation accompanies the superconducting transition.<sup>1,2</sup> This analysis showed a split position for the axial oxygen atom [O(4)], which we related to the motion of the O(4) atom in an anharmonic double-parabolic-well potential. The existence of this split O(4) position has now been confirmed by other groups.<sup>3</sup> This double-well potential shows softening in the vicinity of  $T_c$ .<sup>2</sup> We have interpreted these changes as a result of the coupling between anharmonic phonons, derived from this double-well potential, and the superconducting order parameter. The coupling between anharmonic phonons and electronic degrees of freedom which are involved in the superconductivity leads to predictions of the oxygen isotope effect very different from those of harmonic theories, and in agreement with recent experimental observations.<sup>4,5</sup>

Additional evidence for the existence of O(4)-related lattice instabilities in these materials has been given by several experiments on  $\text{YBa}_2\text{Cu}_3\text{O}_7$  and related compounds.<sup>6-10</sup> Infrared absorption measurements on  $\text{YBa}_2\text{Cu}_3\text{O}_7$  have shown an anomalous frequency shift and a decrease of 80% in the intensity of the  $585\text{-cm}^{-1}$  mode [which involves the Cu(1)-O(4) vibration] in the vicinity of the superconducting transition.<sup>6</sup> Recent photoinduced infrared absorption of local modes of insulating  $\text{YBa}_2\text{Cu}_3\text{O}_6$  and  $\text{Tl}_2\text{Ba}_2\text{Ca}_{1-x}\text{Gd}_x\text{Cu}_2\text{O}_8$  (Ref. 7) suggest a double-well potential structure, in agreement with

the EXAFS results.<sup>1,2</sup> Cu-O(4) elastic anomalies across  $T_c$  have also been found in  $\text{ErBa}_2\text{Cu}_3\text{O}_7$  by ion-channeling experiments.<sup>8</sup>

Direct theoretical support for the existence of anharmonic potentials for the O(4) comes from the interpretation of infrared and Raman experiments<sup>9,10</sup> in terms of charge-transfer models.<sup>11</sup> If the electron-phonon coupling is sufficiently large, the charge-transfer models lead to double-well potentials.<sup>12,13</sup> Such potentials commonly occur in ferroelectric materials that have a perovskite structure analogous to that of  $\text{YBa}_2\text{Cu}_3\text{O}_7$ .<sup>14,15</sup> Several other models also predict a double-well behavior for the motion of the oxygen atoms in these materials.<sup>16-19</sup>

Although such details of the structure of the axial-oxygen site have not been reported by traditional crystallographic measurements, recent pair-distribution function analysis of elastic- and inelastic-neutron-scattering data have shown evidence for a split axial-oxygen position both in  $\text{Tl}_2\text{Ba}_2\text{CaCu}_2\text{O}_8$  and  $\text{La}_{1.85}\text{Ba}_{0.15}\text{CuO}_4$ , supporting our *dynamical* interpretation of this lattice fluctuation.<sup>20</sup>

EXAFS and other local probes such as vibrational spectroscopy can be better than x-ray and neutron diffraction for locating and characterizing small perturbations in local structure, especially for low- $Z$  atoms in materials with complicated structures which are inappropriate for single-crystal neutron-diffraction studies.<sup>21</sup> An additional complication in the interpretation of both diffraction and EXAFS results is the anharmonicity which we have found to be associated with this site.

The effect of lattice vibrations on EXAFS, reflected in the *relative* motion of atomic pairs, is usually taken into

account by the use of a harmonic Debye-Waller factor. However, such treatment is invalid when the atomic vibrations sample anharmonic contributions to the interatomic potentials.<sup>22</sup> For cases of weak to moderate anharmonicity, perturbative treatments in which the first few cumulants to the Debye-Waller factors are retained are applicable.<sup>23,24</sup> However, for systems which exhibit strong anharmonicity (whenever  $k\sigma \sim 1$ , where  $k$  is the photoelectron wave vector and  $\sigma$  the second-order cumulant of the Debye-Waller factor), the cumulant expansion diverges, and it is necessary to consider the effect of anharmonicity in a nonperturbative manner. Examples of this behavior are materials near a structural phase transition, e.g., systems near the melting point.<sup>25</sup> The effect of non-Gaussian radial distribution functions (RDF's) on EXAFS was first discussed by Eisenberger and Brown<sup>26</sup> and Crozier and Seary<sup>25</sup> in the interpretation of the EXAFS of Zn near its melting point. Hayes and Boyce<sup>27</sup> described a general approach in which the RDF is parametrized in terms of variables which were allowed to vary when fitting the calculated EXAFS to experimental data. In this approach the temperature does not enter explicitly in the parameterization of the RDF and, consequently, the effect of the temperature in the atomic vibrations and static disorder cannot be separated. Atomic potentials in the classical limit were subsequently derived from these non-Gaussian RDF's for superionic conductors, illustrating the utility of EXAFS as a probe of interatomic potentials.<sup>28</sup>

We have generalized the derivation of the EXAFS equation, considering a general pair potential describing the relative pair motion, to the finite-temperature quantum regime. This regime contains as limiting cases both the zero-temperature limit and the classical regime. In this approach we consider a RDF directly derived from a model potential, which is parametrized in terms of variables determined from nonlinear least-squares fits between calculated EXAFS and experimental data. This approach permits the treatment of highly anharmonic motion that cannot be addressed using series expansions of the Debye-Waller factor (cumulant expansions).<sup>23,24</sup> For cases in which the interatomic pair-potentials do *not* depend on temperature, this method does not require fitting the RDF at each temperature of interest because, when the potential is determined at a given temperature, the temperature dependence of the RDF follows.<sup>29</sup> Moreover, in the general case (a quantum-mechanical system at finite, nonzero temperature) no explicit analytical relation exists between the RDF and the potential. It is consequently impossible to extract an interatomic potential from determined RDF's.

Because harmonic analysis of the contribution of the axial oxygen to the Cu  $K$ -edge polarized EXAFS in  $\text{YBa}_2\text{Cu}_3\text{O}_7$  failed, we have applied this approach to the determination of the structure of this site. An application of this method for a system in the classical limit has been discussed elsewhere.<sup>30</sup>

Here we present the detailed analysis of polarized Cu-O(4) EXAFS contributions to the Cu  $K$  edge, using RDF's derived from different model potentials including double-parabolic, and single- and double-well  $\phi^4$  poten-

tials. We also present the results of fits using a harmonic Debye-Waller factor, indicating the deficiencies of the harmonic treatment in fitting the experimental data. We discuss the relation between the results obtained and other diffraction and EXAFS studies.

In Sec. II we introduce the general formalism used to analyze EXAFS in anharmonic systems. In Sec. III we discuss the reduction of the EXAFS data and the results of fitting the EXAFS data using a double-parabolic-well potential, a modified  $\phi^4$  potential, and harmonic fits. In Sec. IV we review results of other diffraction and EXAFS studies of the axial oxygen in  $\text{YBa}_2\text{Cu}_3\text{O}_7$  and discuss their relation to the EXAFS results presented in this paper. Finally, in Sec. V, we present a summary of results and conclusions.

## II. ANALYSIS OF EXAFS USING INTERATOMIC POTENTIALS

To calculate the effect of anharmonicity of EXAFS, we start with the standard  $K$ -edge single-scattering EXAFS formula for polarized x rays incident on an oriented sample for the case of a static bond of length  $r$ .<sup>31</sup> The structure of the results will have the same form for absorption from an arbitrary edge in polarized or unpolarized measurements.

$$\chi(k) = -(\hat{\epsilon} \cdot \hat{r})^2 N \text{Im} \left[ B(k, r) \frac{\exp[2ikr + i\psi(k, r)]}{kr^2} \right], \quad (1)$$

where  $\hat{\epsilon}$  denotes the x-ray polarization vector,  $\mathbf{r}$  is the bond vector between absorbing and scattering atoms, and  $N$  is the number of atoms located at a distance  $r$  from the absorbing atom. Here  $k = \sqrt{2(E - E_0)}$  is the photoelectron wave vector in atomic units ( $\hbar = e = m_e = 1$ , these will be used throughout this paper unless otherwise noted) referenced to the arbitrary energy reference,  $E_0$ , e.g., the ionization threshold.  $\psi(k, r)$  denotes the total phase shift  $\psi(k, r) = 2\delta_1(k) + \phi(k, r)$ , with  $\delta_1$  denoting the  $l = 1$  central-atom partial-wave phase shift and  $\phi(k, r)$  the backscattering phase.  $B(k, r)$  is an amplitude factor associated with the backscattering process, which also takes into account inelastic scattering suffered by the photoelectron and the effect of the core-hole relaxation.<sup>32</sup>

To account for the motion of the atomic pair of interest we form a statistical average of  $\chi$  [cf. Eq. (1)],

$$\langle \chi \rangle = \text{Tr}[\rho \chi]. \quad (2)$$

Here  $\rho$  denotes the density matrix associated with the many-body Hamiltonian,  $H(\{q_i\}, \{p_i\})$ , that involves the coordinates,  $\{q_i\}$ , and momenta,  $\{p_i\}$ , of all the ions in the system. We approximate this average assuming that the motion of the pair of interest can be described by a single-particle Hamiltonian,  $h = p^2/2m + V(z)$ , where  $V(z)$  denotes an effective single-particle potential,  $p$  is the relative momentum of the pair,  $z$  denotes the displacement relative to the average pair distance  $R$ , i.e.,  $r = R + z$ , and we consider only motion along the bond direction.  $\chi$  is taken to be an operator due to its dependence on the parameter  $r$ . The statistical average can be expressed in terms of a RDF,  $g(z)$ ,

$$\langle \chi \rangle = \int dz g(z) \chi(k, r(z)), \quad (3)$$

where  $g(z)$  is given in terms of the single-particle wave functions,  $\{\Psi_i(z)\}$ , derived from the Hamiltonian  $h$ :

$$g(z) = \frac{\sum_i |\Psi_i(z)|^2 e^{-\beta \epsilon_i}}{\sum_i e^{-\beta \epsilon_i}}. \quad (4)$$

Here,  $\epsilon_i$  denotes the  $i$ th eigenvalue of the Hamiltonian,  $h$ , and  $\beta = 1/k_B T$ , where  $k_B$  is the Boltzmann constant and  $T$  the temperature of the system. We determine the wave functions  $\{\Psi_i(z)\}$  by solving the Schrödinger equation using the reduced mass,  $m$ , for the atomic pair of interest, and a model potential,  $V(z)$ , characterized in terms of parameters determined by fitting  $\langle \chi \rangle$  to experiment.

Since the variation of the EXAFS phase  $\psi(k, r)$  and amplitude functions  $B(k, r)$  is small in the region of interest of the ionic motion, we approximate Eq. (3) by

$$\langle \chi \rangle = -(\hat{\epsilon} \cdot \hat{r})^2 N \operatorname{Im} \left[ B(k, R) e^{i\psi(k, R)} \times \int dz g(z) \frac{e^{2ikr}}{kr^2} \right]. \quad (5)$$

This allows us to use EXAFS amplitudes and phases derived from reference systems.<sup>33</sup>

Due to the reduction of the many-body problem, required to evaluate Eq. (2) to the single-particle average defined by Eqs. (3) and (4), the effective single-particle potential,  $V(z)$ , may exhibit temperature dependence.<sup>29</sup> In addition, in cases in which degrees of freedom other than the ionic ones, e.g., electronic degrees of freedom, exhibit significant changes in the temperature range of interest, the effective single-particle potential obtained after integrating out these other degrees of freedom will exhibit temperature dependence. This is the case in the analysis of O(4) in  $\text{YBa}_2\text{Cu}_3\text{O}_7$  across the superconducting transition (see Sec. III). Since  $V(z)$  represents the effect of all surrounding atoms in the relative motion of the pair, any correlations between different pairs are neglected. In this sense this treatment is analogous to the Einstein approximation commonly used in EXAFS analysis. Also, the fact that we only consider effective pair potentials implies that the properties derived from different pairs, even when one atom is involved in both pairs, will be different (see Sec. III).

Equations (4) and (5) represent the average of  $\chi$  for the most general case of a quantum system at finite nonzero temperature. In several applications, e.g., materials near the melting point,<sup>30</sup> however, all temperatures of interest are far above the lowest-energy eigenvalues of  $h$  ( $T \gg \epsilon_0$ ). In this case a simpler classical treatment can be used, where the RDF is given by

$$g(z) = e^{-\beta V(z)} / \left[ \int dz e^{-\beta V(z)} \right]. \quad (6)$$

The RDF gives a complete description of the pair motion and one can extract the temperature dependence of any cumulant by calculating the moments of interest,

$$\langle z^n \rangle = \int dz g(z) z^n, \quad (7)$$

allowing the testing of the convergence of cumulant expansions in situations of interest. In the harmonic case,  $V(z) = m\omega_0^2 z^2/2$ , the RDF has a Gaussian shape given by

$$g(z) = \frac{e^{-z^2/\sigma^2(T)}}{\sqrt{\pi\sigma^2(T)}}, \quad (8)$$

where the mean-square fluctuation of the bond length is given by<sup>34</sup>

$$\sigma^2(T) = \coth \left[ \frac{\beta\omega_0}{2} \right] / 2m\omega_0, \quad (9)$$

which, in the classical limit ( $T \gg \omega_0$ ), reduces to  $\sigma^2(T) = 1/\beta m \omega_0^2$ .

Given the calculated  $\langle \chi \rangle$ , defined by Eqs. (4) and (5) [or in the classical regime, Eq. (6)], we perform a non-linear least-squares fit between  $\langle \chi \rangle$  and experimental data in the  $k$  region of interest, using as parameters to be determined  $R$  and the constants which define  $V(z)$ , at a fixed temperature. The number of atoms,  $N$ , is held fixed at the crystallographically determined value. The EXAFS amplitude function and phase functions are determined using reference compounds (if a material with a similar local structure is available), theoretical calculations, or (if the anharmonicity is negligible at low temperatures) the low-temperature data, and then held fixed as a function of temperature. As shown by Eq. (4), in the general case of a quantum system at finite, nonzero temperature there is *no explicit* relation between the RDF,  $g(z)$ , and the potential  $V(z)$ . Consequently, fits between experiment and theory using the parameters that define  $g(z)$  do not yield  $V(z)$  and the *dynamical* information associated with this potential. We note, however, that the parametrization of  $g(z)$  provides a natural way to study non-Gaussian static disorder, as commonly encountered in materials that undergo rapid annealing. In this case, one can still use Eq. (5), with  $g(z)$  characterized in terms of parameters determined by fitting Eq. (5) to experimental data.

The usable region of EXAFS data is typically  $k \geq 2.5 \text{ \AA}^{-1}$ , since, at lower energies, the x-ray-absorption signal is usually dominated by multiple scattering and transitions to bound states, and chemical effects limit the transferability of the EXAFS amplitude and phase functions. Consequently, information about the large distance behavior of the RDF,  $|z| \geq 0.4 \text{ \AA}$ , is lost in the standard EXAFS analysis.<sup>27</sup> The method described above provides a reconstruction of this large-distance behavior of the RDF, using the available EXAFS data, data from other experimental probes, i.e., coordination numbers derived from crystallographic studies, and functional forms for the potential suggested by other physical properties. The application of this method is then limited by the availability of this extra information, as fits in which the coordination numbers are allowed to vary and the potential has a general form can lead to convergence to the experimental spectra but result in unphysical potentials. However, we note that, given accurate information about coordination numbers and reliable reference amplitudes,

this method leads to a precise characterization of the potential. As discussed in Sec. III, this method allowed us to discriminate between different double-well potentials for the motion of O(4) in  $\text{YBa}_2\text{Cu}_3\text{O}_7$ , indicating that a double-parabolic-well potential was more adequate than the  $\phi^4$  potential commonly encountered in ferroelectrics.<sup>14</sup> It is also important to mention that this method provides *dynamical* information about the motion of the atoms contained in the eigenvalue spectrum of the pair potential.

We finally note that the applicability of this method is not restricted to systems of high anharmonicity, where the cumulant expansion breaks down ( $k\sigma \sim 1$ ), and actually provides a way to test the validity of the cumulant expansion in situations of moderate anharmonicity.

### III. ANALYSIS AND INTERPRETATION OF EXAFS RESULTS

Sample characteristics and data acquisition procedures of these measurements have been previously discussed.<sup>1</sup> Here we discuss the reproducibility and accuracy of the data, uncertainties in the interpretation introduced by “leaks” from higher shells in the Fourier-filter isolation of the Cu-O(4) signal and misorientation of the sample, and the results of the fits using different model potentials, including harmonic fits to the data. The temperatures covered in this analysis are  $T_{\text{nom}} = 9, 10, 83, 86, 88, 95,$  and  $105$  K, where  $T_{\text{nom}}$  is the measured temperature of the cold finger and may be  $\sim 5$  K lower than the temperature of the sample. In  $\text{YBa}_2\text{Cu}_3\text{O}_7$ ,<sup>35</sup> the  $\text{CuO}_3$  chains are composed of Cu(1) and O(1,4) where O(4) is the axial oxygen with Cu(1)-O(4)  $\sim 1.87$  Å and Cu(2)-O(4)  $\sim 2.29$  Å. The joint contribution of the Cu(1)-O(4) and Cu(2)-O(4) pairs lies in the region  $\sim 1 \leq R \leq 2$  Å, where two peaks are discernible in the plot of the Fourier transform (Fig. 1). After normalization and background subtraction of the absorption coefficient,  $\mu(E)$ , the Fourier transform was obtained by weighting the total EXAFS signal with a factor  $k^3$ . Several fits to the background were tried until the background residual in the Fourier transform, i.e., the contribution for  $r \leq 0.5$  Å, was minimized. The  $k$ -space range used in the Fourier transform was  $1.74 \leq k \leq 14.94$  Å<sup>-1</sup> (in all Fourier transforms square windows were used),<sup>36</sup> where the photoelectron momentum,  $k$ , was defined with respect to  $E_0 = 9000$  eV (the inflection point of the first feature in Cu-metal  $K$  edge being 8980.3 eV). The EXAFS signal from the Cu(1)-O(4) and Cu(2)-O(4) pairs was obtained by Fourier filtering—e.g., back transforming over the range in real space  $\sim 1.1 \leq r \leq 2.0$  Å, using square windows in the process (Fig. 1).

The isolated EXAFS signal exhibits a “beat” near  $k = 12$  Å<sup>-1</sup> for temperatures outside a fluctuation region (Fig. 2). This beat indicates the presence of two waves from shells at different distances. The rapid damping of the Cu(2)-O(4) signal<sup>2,38</sup> implies that the origin of this beat is not destructive interference of the Cu(1)-O(4) and Cu(2)-O(4) signals. However, the presence of a beat at  $k \sim 3$  Å<sup>-1</sup> and the maximum in the amplitude at  $k \sim 7.5$  Å<sup>-1</sup> result from interference between the Cu(1)-O(4) and

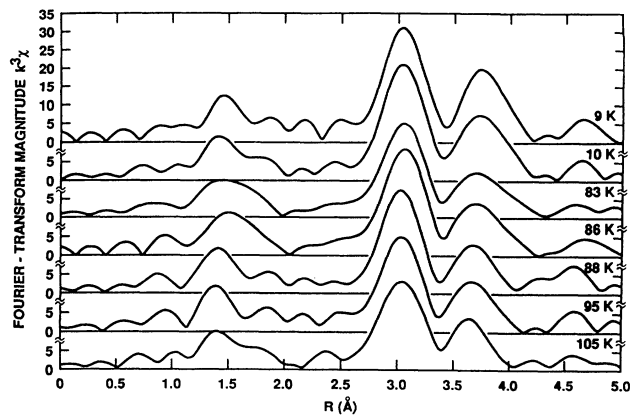


FIG. 1. Fourier-transform moduli of the EXAFS of oriented  $\text{YBa}_2\text{Cu}_3\text{O}_7$   $\hat{\epsilon}||c$  at (from top to bottom) 9, 10, 83, 86, 88, 95, and 105 K. The transform range is  $k = 1.74\text{--}14.94$  Å<sup>-1</sup> (square windows were used). The contribution of the Cu-O(4) pairs is observed at  $R = 1.1\text{--}2.0$  Å. (Note the different structure of the 83- and 86-K spectra). The peak near  $R = 3.1$  Å contains the contributions of the Cu(2)-Y, [Cu(1)+Cu(2)]-Ba, and Cu(2)-Cu(2) and the peak near 3.7 Å contains the Cu(1)-Cu(2) signal.

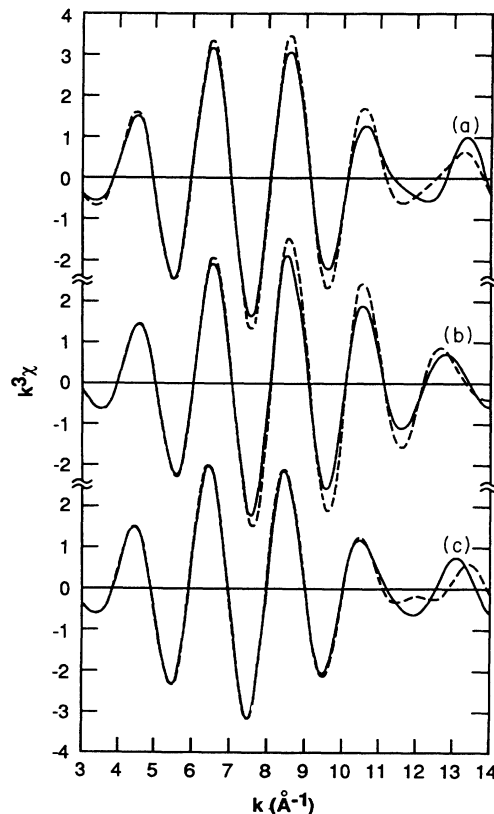


FIG. 2. Comparison of Fourier-filtered data from individual runs on the same sample taken at different times. In all cases the transform range is  $k = 1.74\text{--}14.94$  Å<sup>-1</sup> (square windows were used), the backtransform range is  $R = 1.1\text{--}2.0$  Å. (a) 10 K, (b) 86 K, (c) 105 K. Note that, although there are noticeable difference in the amplitude, the phase difference over the whole  $k$  range is very small.

Cu(2)-O(4) signals, with these bond lengths differing by  $\Delta R \sim 0.42$  Å. This is shown in Fig. 3, where the individual Cu(1)-O(4) and Cu(2)-O(4) obtained in the fits of Ref. 2, which use a double-parabolic-well potential, are plotted, indicating that, for  $k > 11$  Å<sup>-1</sup>, the Cu(2)-O(4) contributes to less than 10% to the total Cu-O(4) signal. From these observations we conclude that the origin of this beat is associated with two O(4) positions separated by  $\sim 0.13$  Å.

The reproducibility and implied high level of accuracy of this data over the entire  $k$  range is demonstrated by the Fourier-filtered signal from individual runs taken at the same temperature (Fig. 2). The level of reproducibility can also be inferred by the very small difference in the resulting fitting parameters, between data at  $T_{\text{nom}} = 9$  and 10 K, as these two data sets were collected on different beam lines under different operating conditions. (See Tables I and II.) In order to quantify the effect of noise and other systematic errors in the data, we averaged all the data with a beat present (data outside the fluctuation region) and calculated the standard deviation of each individual set at each temperature. From this standard deviation the probability that the absence of a beat at temperatures  $T_{\text{nom}} = 83$  and 86 K was due to noise was calculated to be less than 0.5%.

It is important to accurately characterize the orientation of the sample in order to ensure that the two observed distances do not contain contributions from Cu-equatorial-oxygen bonds. This was accomplished by x-ray diffraction and pole-figure analysis. In Fig. 4 we present a pole-figure scan of the (012) peak in the polar direction resulting from averaging four different azimuthal-angle scans. This figure shows that more than 96% of the particles in the sample are oriented with the  $c$  axis within 5° of the  $z$  axis (assuming a Gaussian peak shape, not including the instrumental linewidth of 3°). Unlike normal diffraction patterns, the pole-figure scan reflects the actual distribution of orientations about the  $c$  axis.<sup>37</sup> This leads to an upper limit of equatorial oxygen contributions in the EXAFS signal for  $\hat{\epsilon} \parallel c$  of less than 2%. The  $> 90\%$  polarization of the beam is then the limiting factor on the Cu-equatorial-oxygen contributions, which are thus  $< 10\%$ , are much smaller than the  $\sim 50\%-50\%$  ratio for the peak heights corresponding to the two O(4) sites obtained from fits to the data using a double-parabolic-well potential (see below).<sup>2</sup>

We estimated contributions from the Cu(2)-Y, [Cu(1)+Cu(2)]-Ba, and Cu(2)-Cu(2) shells to the main fre-

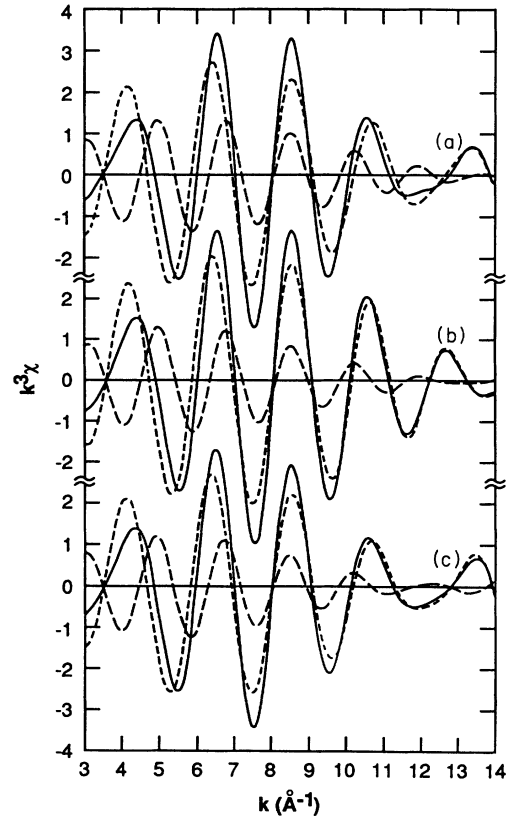


FIG. 3. EXAFS fits using the double-parabolic-well potential  $V(z)$  defined in Eq. (10): solid line, total Cu(1)-O(4)+Cu(2)-O(4) contribution; dotted line, Cu(1)-O(4) contribution; dashed line, Cu(2)-O(4) contribution at (a) 10 K, (b) 86 K, and (c) 105 K.

quency range of the axial oxygen by performing a multiple-shell fit using theoretical EXAFS phases and amplitudes, and the Cu(1)-O(4)-Cu(2) single- and multiple-scattering contribution were modeled using empirical parameters derived from  $\text{La}_2\text{CuO}_4$ .<sup>39,40</sup> We filtered these contributions using the same ranges used for the isolation of the O(4) contribution. As seen in Fig. 5, the effect of these contributions is negligible in the beat region.

In order to compare anharmonic fits obtained using a double-parabolic-well potential<sup>2</sup> with fits using other potentials we show these double-parabola fits in Fig. 6, and the RDF,  $g(z)$ , and potential  $V(z)$  in Fig. 7. We note that, although the RDF shows a double-peak structure,

TABLE I. Cu(1)-O(4) parameters resulting from the fit to  $\hat{\epsilon} \parallel c$  EXAFS data.

$T_{\text{nom}}$ (K)	$R + z_1$ (Å)	$R + z_2$ (Å)	$a_1$ ( $10^6$ K/Å <sup>2</sup> )	$b_1$ ( $10^6$ K/Å <sup>2</sup> )	$\hbar\omega_T$ (K)	$\Delta E_0$ (eV)
9	1.821	1.954	1.92	1.98	151	6.5
10	1.820	1.955	1.85	1.85	153	6.5
83	1.821	1.941	1.64	1.54	205	4.6
86	1.823	1.945	1.51	1.51	274	4.6
88	1.820	1.955	1.85	1.95	157	6.5
95	1.821	1.955	1.91	1.98	137	6.7
105	1.821	1.954	1.89	1.89	155	6.5

TABLE II. Cu(2)-O(4) parameters resulting from the fit to  $\hat{\epsilon}||c$  EXAFS data.

$T_{\text{nom}}$ (K)	$R + z_1$ (Å)	$R + z_2$ (Å)	$a_2$ ( $10^4 \text{ K}/\text{Å}^2$ )	$b_2$ ( $10^4 \text{ K}/\text{Å}^2$ )	$\Delta E_0$ (eV)
9	2.178	2.313	3.45	3.25	6.5
10	2.179	2.312	3.58	3.58	6.5
83	2.176	2.299	3.35	3.35	4.6
86	2.181	2.303	3.48	3.48	4.6
88	2.179	2.313	4.35	3.75	6.5
95	2.183	2.319	4.16	3.62	6.7
105	2.189	2.322	3.88	3.88	6.5

this is not the case for the Fourier transform of the data. This is expected, since the structure of the peaks in the Fourier transform contains broadening introduced by the photoelectron backscattering amplitudes, many-body effects, etc. A similar effect is expected in Fourier density maps obtained from diffraction measurements, as those peaks are broadened by the inherent width of scattering factors (in x-ray diffraction), instrumental resolution, etc. The form of the potential,  $V(z)$ , used in these fits is

$$V(z) = \frac{a}{2}(z - z_1)^2, \quad z \leq z_0, \quad (10)$$

$$\frac{b}{2}(z - z_2)^2, \quad z \geq z_0,$$

where  $z_0$  is determined by the continuity condition  $V(z_0^+) = V(z_0^-)$ . We fit the EXAFS from this potential as described in Sec. II, over the range  $k = 3 - 14 \text{ Å}^{-1}$  on the Fourier-filtered data. Fitting over a region  $1 \text{ Å}^{-1}$  less than the transform range at both ends avoids distortions introduced by the filtering procedure at the edges of the filtering region. The ten parameters determined by the fit were  $E_0$ , and the potential parameters  $a$ ,  $b$ ,  $R + z_1$ ,  $R + z_2$ , for each bond, i.e., Cu(1)—O(4) and Cu(2)—O(4) (Tables I and II).<sup>2</sup> The temperature-independent EXAFS amplitude,  $B(k, R)$ , and phase,  $\psi(k, R)$ , functions were obtained from the EXAFS of Cu—O bonds in the  $a$ - $b$  plane.<sup>1</sup> The number of O(4) atoms at a distance  $R$  from

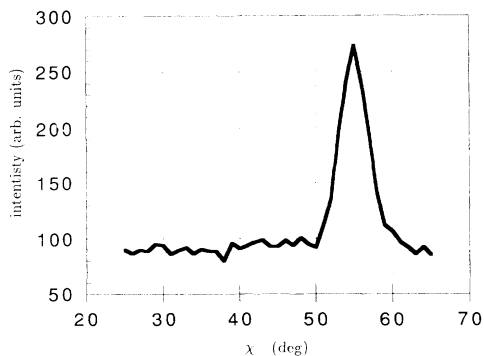


FIG. 4. Pole-figure curve for the (012) peak as a function of the polar angle, trace resulting from averaging four different azimuthal-angle scans, illustrating the degree of orientation of the sample.

Cu(1) was fixed at two. Estimated errors in the resulting parameters were obtained by averaging the values of these parameters outside the fluctuation region ( $T_{\text{nom}} = 83$  and  $86 \text{ K}$ ), and calculating the standard deviation from these average values.<sup>2</sup>

As pointed out in Ref. 2, the most important finding from this fit is that the shape of the Cu-O(4) interatomic potential is a double well with two nearly degenerate levels, with  $\epsilon_1 - \epsilon_0 < 200 \text{ K}$ , separated from higher levels by  $\sim 1500 \text{ K}$ , and minima located  $\sim 0.13 \text{ Å}$  apart. The O(4) motion thus requires a quantum-mechanical description, since only these two vibrational levels are appreciably occupied at the temperatures of interest. The site separation decreases  $0.02 \text{ Å}$  for temperatures inside a fluctuation region  $T_{\text{nom}} = 83 - 86 \text{ K}$ . This change in the potential results in an increase of the interwell tunneling frequency,  $\hbar\omega_T = \Delta\epsilon = \epsilon_1 - \epsilon_0 \sim 80 \text{ K}$  (Fig. 9). The rms fluctuation of the bond length,  $\sigma$ , the Debye-Waller factor in a harmonic treatment, shows a corresponding decrease at  $T_{\text{nom}} = 83$  and  $86 \text{ K}$  [Fig. 10(a)]. Similar decreases in the rms fluctuation from the equilibrium positions of the Cu

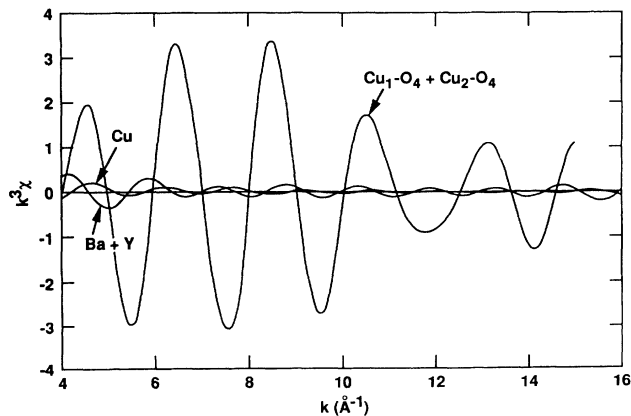


FIG. 5. Contributions from higher shells to the EXAFS at  $88 \text{ K}$ , filtered over the range  $k = 1.1 - 2.0 \text{ Å}^{-1}$ : (i) contributions arising from the peak at  $R = 3.1 \text{ Å}$  (Cu(2)-Y, [Cu(2 + Cu(1))-Ba, Cu(2)-Cu(2)]) calculated using theoretical phase and amplitude functions (Refs. 31 and 32). (ii) Contributions from the peak at  $R = 3.7 \text{ Å}$  single- and multiple-scattering paths involving Cu(1)-O(4)-Cu(2), calculated using amplitude and phase derived from  $\text{La}_2\text{CuO}_4$ .

and axial O atoms have been observed in ion-channeling experiments on  $\text{ErBa}_2\text{Cu}_3\text{O}_7$ .<sup>8</sup>

It is important to note that, as EXAFS measures the average environment around an absorbing atom, the double-well potential is thus a convenient description for the average Cu(1)-O(4) motion. A more realistic model involves a cluster formed by the Cu(1) and the two neighboring O(4) atoms. Exact diagonalization of the model electron-phonon Hamiltonian described in Ref. 9 (which takes into account charge transfer) indicates that, for large enough electron-phonon coupling, the asymmetric vibration of the two O(4) atoms with respect to the Cu(1) (infrared-active mode) develops two degenerate minima leading to the observed RDF using EXAFS.<sup>13</sup> The symmetric vibration (Raman-active mode) of the two O(4) atoms with respect to the Cu(1) does not show a double-well behavior even for strong electron-phonon coupling. This behavior might explain the apparently contradictory observations of the anomalous behavior described above for the infrared-active  $585\text{-cm}^{-1}$  mode,<sup>6</sup> and the suggestion of harmonic behavior from Raman measurements of the  $505\text{-cm}^{-1}$  mode.<sup>41</sup> It also explains the derivation of a nearly symmetric RFD and associated double-well potential from EXAFS,<sup>2</sup> in spite of the asymmetric environment around the O(4) atom, i.e., short Cu(1)—O(4) bond and long Cu(2)—O(4) bond.

We also note that the tunnelling frequency  $\omega_T$  was ob-

tained assuming the effective mass of the pair to be given by the reduced Cu(1)-O(4) mass,<sup>2</sup> if the effective mass of the pair is bigger [for example, if the Ba atom is "dragged" by the O(4)] the tunneling frequency will be smaller. In this sense the obtained values represent an upper limit for the tunneling frequency.

In order to check the sensitivity of the results to the exact form of the potentials employed, an alternative potential used in the fits is a modified  $\phi^4$  potential, commonly used to describe transitions in ferroelectrics. This potential is defined as

$$V(z) = \left[ \frac{a}{2}z^2 + \frac{b}{4}z^4 + \frac{c}{\sqrt{2}}z^3 \right] e^{-d|z/2|}. \quad (11)$$

This form of the potential can represent a single-well potential ( $a > 0, b > 0$ ) or a double-well potential ( $a < 0, b > 0$ ). The parameter  $c$  is introduced to account for any asymmetry in the potential. Finally the exponential term is used to avoid the unphysical behavior  $V(z) \rightarrow z^4$ , for large  $|z|$ . A nonlinear least-squares fit in the region  $k = 4\text{--}14 \text{ \AA}^{-1}$  was tried, using, as parameters to be determined,  $R, E_0$  and the potential parameters  $a, b, c, d$ , for both the Cu(1)-O(4) and Cu(2)-O(4) contributions. The number of atoms  $N$  at a distance  $R$ , and the phase function,  $\psi(k, R)$ , obtained from the Cu-O contribution from the  $E_{||ab}$ -plane EXAFS data, were fixed as a function of

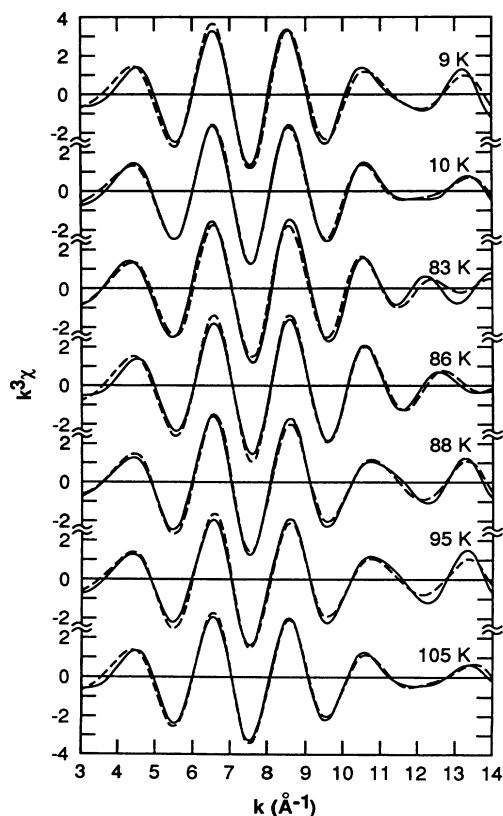


FIG. 6. Comparison between experimental EXAFS spectrum (solid line) and nonlinear least-squares fit obtained using the double-parabolic-well potential  $V(z)$  [Eq. (10)] (dashed line), at  $T = 9, 10, 83, 86, 88, 95,$  and  $105 \text{ K}$ .

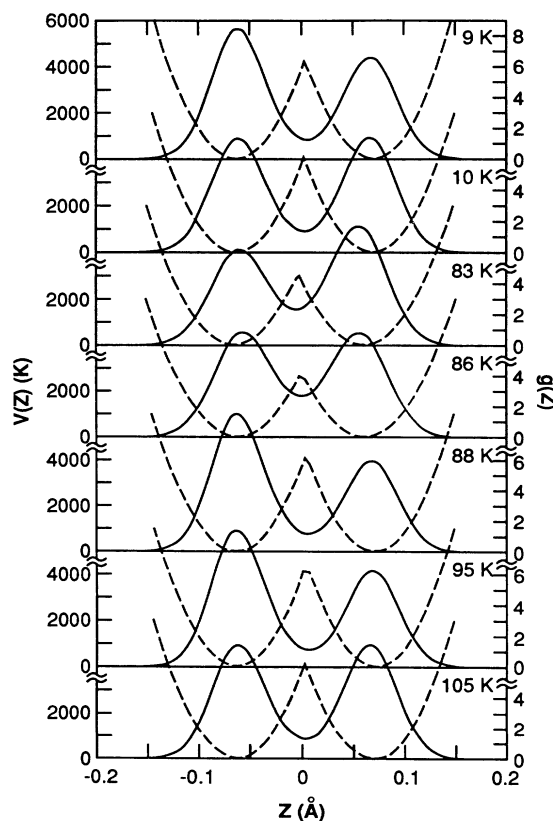


FIG. 7. Radial distribution function,  $g(z)$ , [Eq. (4)] (solid line) and double-parabolic-well potential,  $V(z)$  [Eq. (10)] (dashed line) for  $T = 9, 10, 83, 86, 88, 95,$  and  $105 \text{ K}$ .

temperature. It was *not* possible to fit the data using the amplitude function  $B(k,R)$  derived from the Cu-O contributions from the  $E||ab$ -plane EXAFS data, with attempted fits leading to an amplitude that was  $\sim 50\%$  too small compared with experiment at high values of  $k$ . However, allowing modification to  $B(k,R)$ , it was possible to fit experimental data with an accuracy similar to that obtained using the double parabolic potential [cf. Eq. (10)]. Although the modification needed in the amplitude function  $B(k,R)$  lay outside the range given by the experimental uncertainty, indicating the inadequacy of the  $\phi^4$  potential in describing accurately the motion of the Cu—O(4) bond, this allowed us to check that the conclusions reached in Ref. 2 were independent of the exact form of the potential.

The optimized potential, determined from the non-linear least-squares fit, leads again to two closely spaced levels  $\varepsilon_1 - \varepsilon_0 \sim 200$  K, with higher levels located  $\sim 1200$  K above the first excited-state level  $\varepsilon_1$ . Thus, the motion of the O(4) atom needs to be described quantum mechanically. At all studied temperatures the fits converged to a potential that exhibits a double-well structure [i.e.,  $a < 0$  and  $b > 0$  in Eq. (11)] with a small asymmetry, the well nearer to the Cu(1) site being deeper than the well located farther from the Cu(1) site by about 2% [ $c < 0$  in Eq. (11)]. As was the case for the double-parabolic-well potential for  $T_{\text{nom}} = 83$  and 86 K, the separation between the two minima of the double well decreases by  $\sim 0.02$  Å (Fig. 8). In this case, however, the system is not in a deep double-well potential ( $\varepsilon_0 \sim$  potential barrier height) and although the quantity  $\varepsilon_1 - \varepsilon_0$  shows a similar increase to that obtained in the fits using the double-parabolic-well potential (Fig. 9), it can no longer be interpreted as the tunnelling frequency between the two well minima. In fact, in the fluctuation region the RDF becomes single peaked (Fig. 8).

A figure of merit used to decide the accuracy of these fits was to compare the predicted Cu(1)-Cu(2) distance with that obtained crystallographically. In these fits the Cu(1)-Cu(2) distance, calculated using the average Cu(1)-O(4) and Cu(2)-O(4) distances [ $d_{\text{Cu(1)-Cu(2)}} = d_{\text{Cu(1)-O(4)}} + d_{\text{Cu(2)-O(4)}}$ ], differs by  $\sim 0.06$  Å from the crystallographically determined values.<sup>35</sup> For comparison, fits using the double-parabolic-well potential lead to an error in the Cu(2)-Cu(1) distance of less than  $0.015$  Å.<sup>2</sup>

The EXAFS were also fit assuming harmonic contribution from the Cu(1)—O(4) and Cu(2)—O(4) bonds. It was not possible to achieve reasonable fits using as floating parameters  $r$ ,  $\sigma$ , and  $E_0$  for each shell and fixing the coordination number  $N$  to the crystallographically determined values. Allowing the coordination number  $N$  of each shell to vary led to fits comparable to those generated using anharmonic potentials. As illustrated by Fig. 10(a), the values of  $\sigma$  for the Cu(1)-O(4) pair show unphysical behavior in terms of random variations. Also, the value of the energy reference shift,  $\Delta E_0$ , shows a random trend and variations of the order of 8 eV that lie outside physical expected ranges [Fig. 10(b)]. Finally, the calculated Cu(2)-Cu(1) distance, adding the Cu(2)-O(4) and Cu(1)-O(4) distances, is in error by more than 0.1 Å with respect to crystallographically determined values

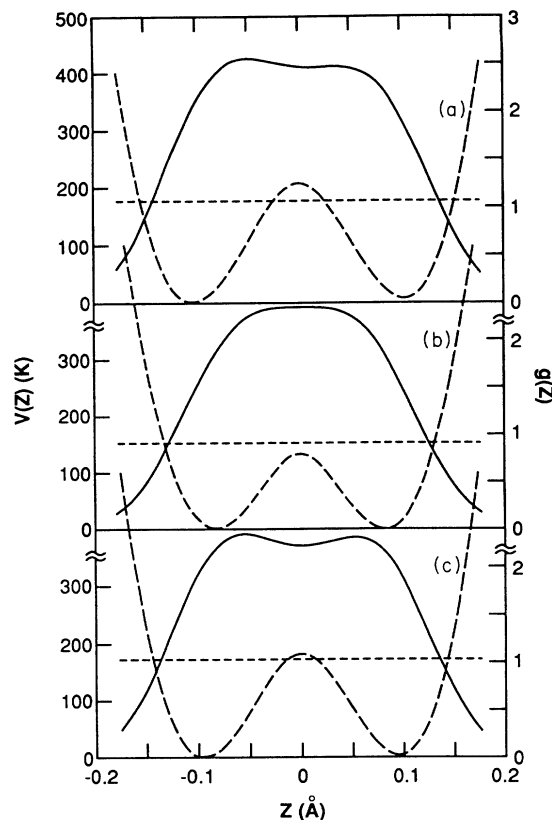


FIG. 8. Radial distribution function,  $g(z)$ , and modified  $\phi^4$  potential,  $V(z)$ , [Eq. (11)] at (a)  $T = 10$  K, (b)  $T = 86$  K, and (c)  $T = 105$  K. The position of the ground-state energy level  $\varepsilon_0$  is indicated by the dashed horizontal line.

[Fig. 10(c)]. These results demonstrate the inadequacy of the harmonic treatment of the Cu-O(4) contributions to the EXAFS. In these harmonic fits the error bars in the resulting parameters were estimated as in the case of the double-parabolic-well fits.

From the three different fits described above, one can conclude that the double-parabolic-well potential is the one that leads to the most consistent results. These fits also illustrate the sensitivity of EXAFS as a tool to deter-

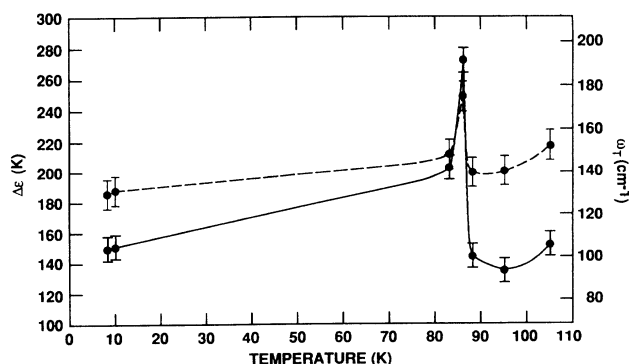


FIG. 9. Energy difference,  $\Delta\varepsilon = \varepsilon_1 - \varepsilon_0$ , between the first excited and ground states of the double-well potential for double-parabolic-well potential [Eq. (10)], solid line; modified  $\phi^4$  potential [Eq. (11)] dashed line.

mine interatomic potentials: The double-parabolic-well potential and the  $\phi^4$  potential, although qualitatively similar, lead to distinctly different EXAFS fits.

In the anharmonic fits in the quantum regime, the position of the energy levels,  $\epsilon_i$ , depends on the assumed mass. In all cases we identified the mass with the reduced Cu-O(4) pair mass. We note, however, that the reduction of the many-body problem to single-particle average, described in Sec. II, implies that the effective mass might be different from the bare reduced mass of the pair,  $m_0$ . In order to test the sensitivity of our results to changes in the mass, we used the mass  $m$  as an additional fitting parameter for the double-parabolic-well potential fits. We found that the mass converged to values  $\sim 1.2m_0$ , resulting in changes in the tunneling frequency on the order of  $\sim 10$  K, when all the other potential parameters are allowed to vary as well. The changes are within the error uncertainties in the values of  $\omega_T$  obtained in fits where  $m = m_0$ .<sup>2</sup> We note that these variations in  $\omega_T$  are different from the ones obtained for a *fixed* potential and changing the value of the mass. In this case the expected exponential isotope effect dependence of the tunneling frequency is obtained as a function of mass.<sup>14</sup>

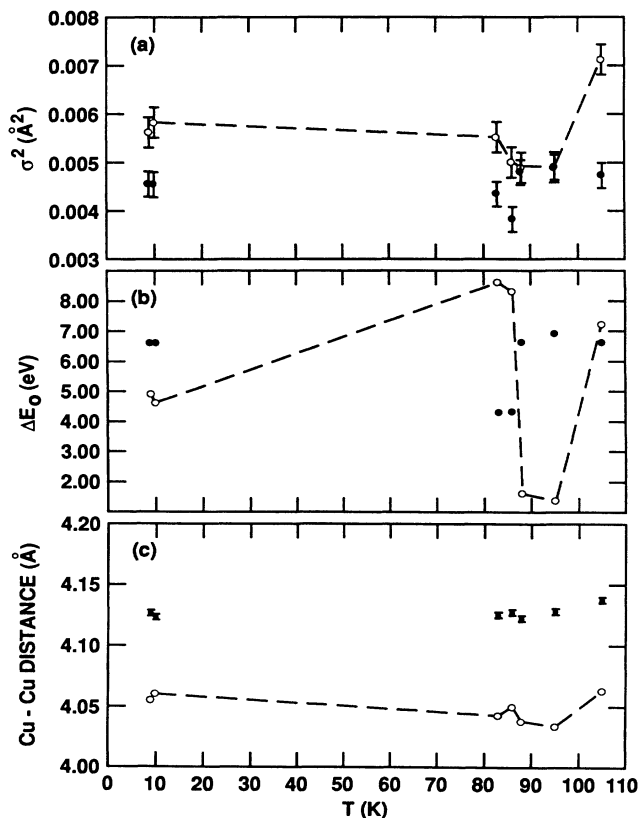


FIG. 10. (a) Debye-Waller factor,  $\sigma$ , for the Cu(1)-O(4) pair, (b) energy reference shift,  $\Delta E_0$ , for the same pair, and (c) Cu(1)-Cu(2) distance, obtained from harmonic fits (open circles), fits using a double-parabolic-well potential (solid circles). The procedure to estimate error bars is described in the text. The dashed line joining the points obtained using harmonic fits illustrates the random variants of these parameters

We have interpreted the observed changes in the tunneling frequency as a result of the coupling between a Hamiltonian describing a two-level system, with energy levels  $\epsilon_0$  and  $\epsilon_1$ , and the superconducting degrees of freedom, described phenomenologically by a Ginzburg-Landau free energy.<sup>2</sup> In order to explain these changes we find it necessary to introduce a coupling of the elastic degrees of freedom not only to the mean-field value of the superconducting order parameter, but also to its fluctuations. While in normal superconductors this fluctuation region is very small, in the high-temperature materials it extends several K around  $T_c$ .<sup>42</sup> We note that the observed changes are *not* directly driven by temperature, but rather are a result of the coupling of the electronic degrees of freedom involved in the superconducting transition and the elastic degrees of freedom leading to the potential describing the ionic motion.

#### IV. COMPARISON OF DEFFRACTION AND EXAFS RESULTS

In EXAFS, the complementary variable to  $r$  is the change in momentum of the photoelectron after back-scattering,  $2k$ . This is the equivalent variable to the momentum transfer,  $q$ , in diffraction experiments. Typical ranges of usable data in EXAFS are  $2.5 \leq k \leq 9-14 \text{ \AA}^{-1}$  for light backscattering elements like oxygen, and up to  $k = 20 \text{ \AA}^{-1}$  for heavy elements such as barium. Consequently, EXAFS provides details about the short-range structure of the RDF that require the analysis of diffraction peaks at high values of  $q$  ( $> 25 \text{ \AA}^{-1}$ ). EXAFS experiments in  $\text{YBa}_2\text{Cu}_3\text{O}_7$  have analyzed the oxygen contribution to Cu K-edge absorption in the range  $3-4 \leq k \leq 12.5-14 \text{ \AA}^{-1}$ , thus providing details of the oxygen RDF on a scale of  $r \sim 0.11 \text{ \AA}$ .<sup>2,43,44</sup> To achieve a similar resolution in discerning nuances in the RDF on this scale using diffraction experiments would require the analysis of data for  $q \sim 25-28 \text{ \AA}^{-1}$ . Because of this inherently higher momentum-transfer upper limit, EXAFS is advantageous in discerning fine details of the local structure that diffraction methods include in the thermal parameters.<sup>27</sup> It is therefore not surprising, especially in this case (weak scatterer for x-ray diffraction and powder samples for neutron diffraction), that EXAFS identifies details in the local structure that have not been observed using traditional crystallographic methods.<sup>35,45</sup> On the other hand, many-body effects, chemical transferability, and multiple scattering limit the range of photoelectron momentum transfer in EXAFS to  $k \geq 2-3 \text{ \AA}^{-1}$ . Because it is precisely this low- $k$  region ( $k \rightarrow 0$ ) which is capable of yielding definitively the coordination number  $N$  and the average nearest-neighbor distance  $R$ , diffraction methods determine the centroid positions of atoms and coordination numbers with greater accuracy than EXAFS.

In x-ray-diffraction experiments, the position of the O(4) atom is the one determined with the greatest uncertainty.<sup>35</sup> This is due in part to the difficulty of accurately resolving the position of a low- $Z$  scattering atom embedded in a matrix of heavy metal atoms, but might also point out to anharmonic motion of this atom. Deter-

minations of the Cu(1)-O(4) distance vary from 1.78 (Ref. 46) to 1.86 Å in most recent measurements.<sup>47</sup> We note that, although the individual Cu(1)-O(4) and Cu(2)-O(4) distances determined from the EXAFS fits, using double-parabolic-well potentials, in Sec. III differ by  $\sim 0.02\text{--}0.03$  Å from the crystallographic values, the Cu(1)-Cu(2) distance determined from our EXAFS results differs by less than 0.01 Å from the reported crystallographic distances.<sup>35,46,47</sup> Although no changes in the local Cu-O(4) structure have been reported in x-ray-diffraction studies, recent high-resolution x-ray-diffraction studies in untwinned single crystals of  $\text{YBa}_2\text{Cu}_3\text{O}_7$  have found discontinuities in the  $c$  lattice parameter across the superconducting transition.<sup>48</sup>

Neutron powder diffraction experiments, which tend to be more sensitive to the position of oxygen atoms, measure a Cu(1)-O(4) distance similar to that obtained using x-ray diffraction. However, the Rietveld technique is not well suited to determining anisotropic thermal motion.<sup>46</sup> It is interesting to note that, in some refinements, a split position of the O(4) was assumed, giving a somewhat better agreement factor.<sup>46</sup> Neutron-diffraction studies<sup>45</sup> of the Cu-O(4) motion have reported no change in the average Cu-O(4) distances across  $T_c$  and no evidence in the Fourier density plot for a split O(4) position on a scale  $\geq 0.35$  Å. The results present in Sec. III are consistent with these findings, as we do not observe a change of the average Cu—O(4) bond lengths, and the separation of the two well sites is *only* 0.13 Å.

It is important to note, however, that in recent pair-distribution function analysis of elastic- and inelastic-neutron-scattering data, a split axial-oxygen position has been reported in  $\text{Ti}_2\text{Ba}_2\text{CaCu}_2\text{O}_8$  and  $\text{La}_2\text{CuO}_4$ .<sup>20</sup> These studies indicate that the nature of this distortion is *dynamic* (as assumed in our EXAFS analysis) and, consequently, might not be detectable by elastic-neutron-diffraction studies, even by increasing their sensitivity.

In EXAFS, each near-neighbor atom gives a unique signal that can be separated from contributions of the other atoms to the spectrum when their positions differ by more than  $\Delta R > 1/k_{\text{max}}$ , where  $k_{\text{max}}$  is the maximum value of  $k$  available in the data. This feature is enhanced by the polarized XAS measurements on the oriented  $\text{YBa}_2\text{Cu}_3\text{O}_7$  samples.<sup>2,38</sup> In EXAFS experiments carried out in polycrystalline unoriented samples,<sup>43,49</sup> it is not possible to directly resolve by Fourier filtering of the data the O(4) signal from that originating from other oxygen atoms, since their separations are within a range  $\sim 0.1$  Å. However, the Cu(1)-O(4) distance has been determined using curve fits to the experimental EXAFS signal assuming different shells of oxygen atoms. It must be noted, however, that, in the case of unpolarized EXAFS in an unoriented sample, the Cu(1)-O(4) signal corresponds to  $\frac{1}{6}$  the total Cu-O EXAFS signal in the range  $1.85 \leq r \leq 1.95$  Å. Consequently, the accuracy in the determination of parameters is reduced from that obtained in polarized EXAFS experiments. The determined values for the Cu(1)-O(4) distance, assuming harmonic motion for the pair, vary from 1.845 (Ref. 49) to 1.88 Å,<sup>43</sup> consistent

with the Cu(1)-O(4) distance 1.88 Å derive from the weighted average of the Cu(1)-O(4) positions found in Sec. III. Yang *et al.*<sup>38</sup> have performed polarized EXAFS experiments in  $\text{YBa}_2\text{Cu}_3\text{O}_7$ . They analyzed the dependence of the Cu(1)-O(4) EXAFS contribution as a function of temperature ( $10 \leq T \leq 300$  K) in the region of photoelectron momentum  $4 < k < 10$  Å<sup>-1</sup>, finding no significant changes in the average Cu-O(4) distance and Debye-Waller factors. We note, that, in our measurements, the occurrence of *two* Cu(1)-O(4) positions in signaled by the beat in the EXAFS at  $k \sim 12$  Å<sup>-1</sup>.

## V. SUMMARY AND CONCLUSIONS

In summary, we have developed a method to interpret EXAFS data of anharmonic systems. This method is valid both in quantum and classical regimes and leads to precise determination of interatomic potentials, yielding dynamical information associated with these potentials. Using this method we have obtained the temperature behavior of the copper-axial-oxygen radial distribution function from polarized EXAFS measurements. These results illustrate the sensitivity of the EXAFS technique as a tool to determine interatomic potentials, and also demonstrate the necessity of using an analysis that goes beyond the harmonic approximation of the Debye-Waller factor to interpret these data. The anharmonic analysis indicates that the *average* O(4) motion can be described by motion in a double-well potential, leading to the observation of a split position for the O(4) position. This double-well potential naturally appears in the diagonalization of electron-phonon models (that take into account charge transfer and electron-phonon coupling) in O(4)-Cu(1)-O(4) clusters. The results for average distances, Debye-Waller factors, and nearest-neighbor coordination numbers are in good agreement with other EXAFS and diffraction results. The detection of a split position for the O(4) ion can be understood as a result of the increased sensitivity of this experiment that allows the use of high-energy data  $k \geq 10$  Å<sup>-1</sup>. Within a fluctuation region near  $T_c$ , this separation decreases, leading to an increase tunneling between the two well sites. We note that similar effects have been observed in thallium-based and doped 1:2:3 samples.<sup>50,51</sup> Our results are consistent with a coupling between a Ginzburg-Landau free energy and a two-level system describing the O(4) RD in a double-well potential, where coupling to the fluctuations of the order parameter are included.

## ACKNOWLEDGMENTS

We would like to thank Dave Bish, Anthony Rollet, Yizhak Yacoby, Ed Stern, Anette Bussmann-Holder, and John Tranquada for stimulating discussions and critical comments. Data acquisition was done at SSRL, which is funded by the Department of Energy under Contract No. DE-AC03-82ER-1300. This work was supported by the Office of Basic Research of the Department of Energy, Division of Materials Science.

- \*Also at Harrison M. Randall Laboratory of Physics, University of Michigan, Ann Arbor, MI 48109.
- <sup>1</sup>S. D. Conradson, I. Raistrick, and A. R. Bishop, *Science* **248** 1394 (1990).
  - <sup>2</sup>J. Mustre de Leon, S. D. Conradson, I. Batistić, and A. R. Bishop, *Phys. Rev. Lett.* **65**, 1675 (1990).
  - <sup>3</sup>Y. Yacoby, E. A. Stern, M. Qian, and S. M. Heald (unpublished).
  - <sup>4</sup>K. A. Müller, *Z. Phys. B* **80**, 193 (1990). Also, see J. Schreiber and P. Härtwich, *Physica B* **165-166**, 1079 (1990).
  - <sup>5</sup>A. Bussmann-Holder and A. R. Bishop, *Phys. Rev. B* **44**, 2853 (1991).
  - <sup>6</sup>B. Güttler *et al.*, *J. Phys. Condens. Matter* **2**, 8977 (1990).
  - <sup>7</sup>D. Mihailović *et al.*, *Phys. Rev. B* **44**, 237 (1991).
  - <sup>8</sup>R. P. Sharma *et al.*, *Phys. Rev. Lett.* **62**, 2869 (1989).
  - <sup>9</sup>L. Genzel *et al.*, *Phys. Rev. B* **40** 2170 (1989).
  - <sup>10</sup>R. Zamboni *et al.*, *Solid State Commun.* **70**, 813 (1989).
  - <sup>11</sup>I. Batistić *et al.*, *Phys. Rev. B* **40**, 6896 (1989).
  - <sup>12</sup>C. C. Yu and P. W. Anderson, *Phys. Rev. B* **29**, 2165 (1984).
  - <sup>13</sup>J. Mustre de Leon, I. Batistić, A. R. Bishop, S. D. Conradson, and S. Trugman (unpublished).
  - <sup>14</sup>M. E. Lines and A. M. Glass, *Principles and Applications of Ferroelectrics and Related Materials* (Clarendon, Oxford, 1977).
  - <sup>15</sup>A. D. Bruce and R. A. Cowley, *Adv. Phys.* **29**, 219 (1980).
  - <sup>16</sup>K. H. Johnson *et al.*, *Mod. Phys. Lett. B* **3**, 1367 (1989).
  - <sup>17</sup>N. M. Plakida *et al.*, *Europhys. Lett.* **4**, 1309 (1987); J. R. Hardy and J. W. Flocken, *Phys. Rev. Lett.* **60**, 2191 (1988).
  - <sup>18</sup>D. P. Clougherty, K. H. Johnson, and M. E. McHenry, *Physica C* **162-164**, 1475 (1989).
  - <sup>19</sup>Y. Bar-Yam, *Phys. Rev. B* **43**, 359 (1991).
  - <sup>20</sup>T. Egami *et al.*, in *Electronic Structure and Mechanisms of High-Temperature Superconductivity*, edited by J. Ashkenazi and G. Vezzoli (Plenum, New York, in press); B. H. Toby *et al.*, *Bull. Am. Phys. Soc.* **36**, 990 (1991).
  - <sup>21</sup>E. Salje, *Philos. Mag. Lett.* **62**, 277 (1990).
  - <sup>22</sup>J. A. Krumhansl, in *Proceedings in Life Sciences: Protein Structure, Molecular and Electronic Reactivity*, edited by R. Austin *et al.* (Springer-Verlag, New York, 1987).
  - <sup>23</sup>D. Crozier, J. J. Rehr, and R. Ingalls, in *X-Ray Absorption*, edited by D. C. Koningsberger and R. Prins (Wiley, New York, 1988), p. 773.
  - <sup>24</sup>J. M. Tranquada and R. Ingalls, *Phys. Rev. B* **28**, 3520 (1983).
  - <sup>25</sup>E. D. Crozier and A. J. Seary, *Can. J. Phys.* **58**, 1388 (1980).
  - <sup>26</sup>P. Eisenberger and G. S. Brown, *Solid State Commun.* **29**, 481 (1979).
  - <sup>27</sup>J. B. Boyce *et al.*, *Phys. Rev. Lett.* **38**, 1362 (1977); T. M. Hayes and J. B. Boyce, in *Solid State Physics*, edited by H. Ehrenreich, F. Seitz, and D. Turnbull (Academic, New York, 1982), Vol. 37.
  - <sup>28</sup>T. M. Hayes and J. B. Boyce, *J. Phys. C* **13**, L731 (1980).
  - <sup>29</sup>In the case of the analysis of Fe-O contributions in ferrosilicate minerals, we found a temperature-independent potential in the range  $90 \leq T \leq 1100$  K (Ref. 24). However, for systems near a phase transition, the potential usually exhibits strong temperature dependence, then it is necessary to fit the potential at every temperature of interest. This is the case in the analysis presented here.
  - <sup>30</sup>J. Mustre de Leon *et al.*, in *X-Ray Absorption Fine Structure Spectroscopy VI*, edited by S. Hasnain (Ellis and Horwood, Chichester, UK, in press).
  - <sup>31</sup>J. Mustre de Leon *et al.*, *Phys. Rev. B* **39**, 5632 (1989).
  - <sup>32</sup>J. Mustre de Leon, Ph.D. thesis, University of Washington, 1989.
  - <sup>33</sup>This approximation, in fact, neglects the variation of curved-wave corrections in the backscattering amplitude and phase with distance. Even for large-amplitude atomic motion, where  $|r - R| \leq 0.4 \text{ \AA}$ , these variations are only significant for  $k \leq 2-3 \text{ \AA}^{-1}$  (Ref. 26).
  - <sup>34</sup>C. Cohen-Tannoudji, B. Diu, and F. Laloe, *Quantum Mechanics* (Hermann-Wiley, Paris, 1977), Vol. 1.
  - <sup>35</sup>Compare, e.g., J. J. Caponi *et al.*, *Europhys. Lett.* **3**, 1301 (1987); M. A. Beno *et al.*, *Appl. Phys. Lett.* **51**, 57 (1987); A. Williams *et al.*, *Phys. Rev. B* **37**, 7960 (1988).
  - <sup>36</sup>The use of Gaussian windows was tested, revealing that the effects on the curve-fitting results were not significant.
  - <sup>37</sup>J. S. Kallend, R. B. Schwartz, and A. D. Rollet (unpublished).
  - <sup>38</sup>C. Y. Yang *et al.*, *Phys. Rev. B* **38**, 6568 (1988).
  - <sup>39</sup>B. -K. Teo and P. A. Lee, *J. Am. Chem. Soc.* **101**, 2815 (1979). Even though these amplitudes and phases are not accurate enough to extract coordination numbers with an accuracy of better than 60% and distances better than 0.03 Å, they lead to reliable estimations of the overall contributions of these higher shells. We have reproduced this calculation using the program FEF (Ref. 40), finding variations in bond lengths  $\sim 0.02 \text{ \AA}$ , and in coordination numbers  $\sim 20\%$ .
  - <sup>40</sup>J. J. Rehr, J. Mustre de Leon, S. Zabinsky, and R. C. Albers, *J. Am. Chem. Soc.* **113**, 5135 (1991); J. Mustre de Leon, J. J. Rehr, S. I. Zabinsky, and R. C. Albers, *Phys. Rev. B* **44**, 4146 (1991).
  - <sup>41</sup>G. Burns, F. H. Dacol, C. Feild, and F. Holtzberg, *Solid State Commun.* **75**, 893 (1980).
  - <sup>42</sup>A. J. Millis and K. M. Rabe, *Phys. Rev. B* **38**, 8908 (1988); H. Svensmark and L. M. Falicov, *ibid.* **40**, 201 (1989); D. Yoshioka, *J. Phys. Soc. Jpn.* **59**, 2627 (1990).
  - <sup>43</sup>K. Zhang *et al.*, *Phys. Rev. B* **37**, 3375 (1988).
  - <sup>44</sup>Relative changes in the RDF can be detected with a greater accuracy, e.g., changes in the position of the observed beat in Sec. III of  $\Delta k \sim 1 \text{ \AA}^{-1}$  result in changes between the two positions of  $\sim 0.01 \text{ \AA}$ .
  - <sup>45</sup>G. H. Kwei *et al.*, *Physica C* **169**, 217 (1990).
  - <sup>46</sup>T. Siegrist *et al.*, *Phys. Rev. B* **35**, 7137 (1987).
  - <sup>47</sup>P. Marsh *et al.*, *Phys. Rev. B* **38**, 874 (1988).
  - <sup>48</sup>H. You, U. Welp, and Y. Fang, *Phys. Rev. B* **43**, 3660 (1991).
  - <sup>49</sup>H. Maruyama *et al.*, *Physica C* **160**, 524 (1989).
  - <sup>50</sup>J. Mustre de Leon *et al.*, in *Electronic Structure and Mechanisms of High-Temperature Superconductivity*, edited by J. Ashkenazi and G. Vezzoli (Plenum, New York, in press); P. G. Allen *et al.*, *Phys. Rev. B* **44**, 9480 (1991).
  - <sup>51</sup>J. Mustre de Leon *et al.*, *Phys. Rev. B* **44**, 2422 (1991).